The Astrophysical Journal Letters, 978:L34 (8pp), 2025 January 10 https://doi.org/10.3847/2041-8213/ada354

Radial Evolution of MHD Turbulence Anisotropy in Low Mach Number Solar Wind

Xingyu Zhu[1], Gary P. Zank[1,2], Lingling Zhao[1,2], and Ashok Silwal[1]
[1] Center for Space Plasma and Aeronomic Research (CSPAR), The University of Alabama in Huntsville, Huntsville, AL 35805, USA; xz0017@uah.edu
[2] Department of Space Science, The University of Alabama in Huntsville, Huntsville, AL 35805, USA
Received 2024 September 11; revised 2024 December 20; accepted 2024 December 20; published 2025 January 8

Abstract

The Parker Solar Probe (PSP) and Wind spacecraft observed the same plasma flow during PSP encounter 15. The solar wind evolves from a sub-Alfvénic flow at 0.08 au to become modestly super-Alfvénic at 1 au. We study the radial evolution of the turbulence properties and deduce the spectral anisotropy based on the nearly incompressible (NI) MHD theory. We find that the spectral index of the z^+ spectrum remains unchanged (~ -1.53), while the z^- spectrum steepens, the index of which changes from -1.35 to -1.47. The fluctuating kinetic energy is on average greater than the fluctuating magnetic field energy in the sub-Alfvénic flow while smaller in the modestly super-Alfvénic flow. The NI MHD theory well interprets the observed Elsässer spectra. The contribution of 2D fluctuations is nonnegligible for the observed z^- frequency spectra for both intervals. Particularly, the magnitudes of 2D and NI/slab fluctuations are comparable in the frequency domain for the modestly super-Alfvénic flow, resulting in a slightly concave shape of z^- spectrum at 1 au. We show that, in the wavenumber domain, the power ratio of the observed forward NI/slab and 2D fluctuations is $\sim$15 at 0.08 au, while it decreases to $\sim$3 at 1 au, suggesting the growing significance of the 2D fluctuations as the turbulence evolves in low Mach number solar wind.

Unified Astronomy Thesaurus concepts: Solar wind (1534); Interplanetary turbulence (830); Solar corona (1483); Solar physics (1476)

1. Introduction

Since the first measurement of the sub-Alfévnic solar wind flow (J. C. Kasper et al. 2021; G. P. Zank et al. 2022), Parker Solar Probe (PSP) has gradually accumulated observations of sub-Alfvénic solar wind in the subsequent encounters (L. L. Zhao et al. 2022a; Y. D. Liu et al. 2023; W. Cheng et al. 2024; R. Chhiber et al. 2024). During encounter 15 between 2023 March 16/11:54:58 and 2023 March 17/05:57:20, PSP observed a long period of sub-Alfvénic solar wind over a heliocentric distance R ranging from $15.6R_\odot$ to $22R_\odot$, where $R_\odot$ is the solar radius. The source region of this particular interval may lie in a peripheral region of a coronal hole (W. Cheng et al. 2024) or a midlatitude active region (T. Ervin et al. 2024). A velocity-varying ballistic propagation analysis demonstrated that the same flow is later observed by the Wind spacecraft at 1 au (T. Ervin et al. 2024). The interval observed by Wind has only a modestly super-Alfvénic Mach number $M_A = V_R/V_A$, thanks to the extremely low number density. Here, V_R is the radial component of the solar wind velocity, and V_A is the Alfvén speed.

A general consensus exists that turbulent fluctuations play a significant role in the heating and acceleration of the near-Sun solar wind (W. H. Matthaeus et al. 1999; A. Verdini et al. 2009; S. R. Cranmer & A. A. van Ballegooijen 2012; M. Shoda et al. 2018; G. P. Zank et al. 2018; B. D. G. Chandran & J. C. Perez 2019; L. Adhikari et al. 2020; G. P. Zank et al. 2021; R. Meyrand et al. 2023). Observations throughout the inner heliosphere suggest that MHD turbulence possesses intrinsic variance and spectral anisotropy (W. H. Matthaeus et al. 1990; J. W. Bieber et al. 1996; T. S. Horbury et al. 2008; J. He et al. 2013; D. Duan et al. 2020; X. Zhu et al. 2020; L. L. Zhao et al. 2022b). The nearly incompressible (NI) MHD theory derives the turbulence as a superposition of majority 2D fluctuations and minority NI/slab fluctuations in the plasma beta $\beta_p \ll 1$ or $\sim$1 regimes (G. P. Zank & W. H. Matthaeus 1992, 1993; G. P. Zank et al. 2017). The NI/slab component includes both a dominant quasi-2D component and a minority parallel propagating Alfvén waves as well as magnetosonic fluctuations (G. P. Zank et al. 2020). Such a decomposition is different from the standard "2D+slab" model (J. W. Bieber et al. 1996), which constrains the wavevector parallel or perpendicular to the mean magnetic field.

In the sub-Alfvénic or modestly super-Alfvénic solar wind (low Mach number regime), the measured fluctuating time series is a mix of temporal and spatial variations. The observed spacecraft frequency spectra are an integration of the 4D spectra in the plasma frequency ω and wavenumber $\boldsymbol{k}$ space (L. L. Zhao et al. 2024a, 2024b). Hence, it is inappropriate to derive the spectral anisotropy using the standard Taylor's hypothesis (G. I. Taylor 1938) or modified Taylor's hypothesis (K. G. Klein et al. 2015; S. Bourouaine & J. C. Perez 2018). However, the turbulence properties and its evolution in low M_A flows provide insight into understanding the role of turbulence in solar wind heating and acceleration.

In this Letter, we study in detail the turbulence evolution of a solar wind stream observed by PSP at $R \sim 0.08$ au and Wind at 1 au. Such a "plasma lineup" alignment allows us to trace the radial (time) evolution of the turbulence in an outward-propagating flow as it evolves from sub-Alfvénic to modestly super-Alfvénic. We interpret the observed $z^\pm$ spectra based on the NI MHD theory, which is a superposition model consisting of 2D and NI/slab components. We deduce the inertial-range spectral anisotropy by constructing the wavenumber spectra for each NI turbulence component from the observed spacecraft

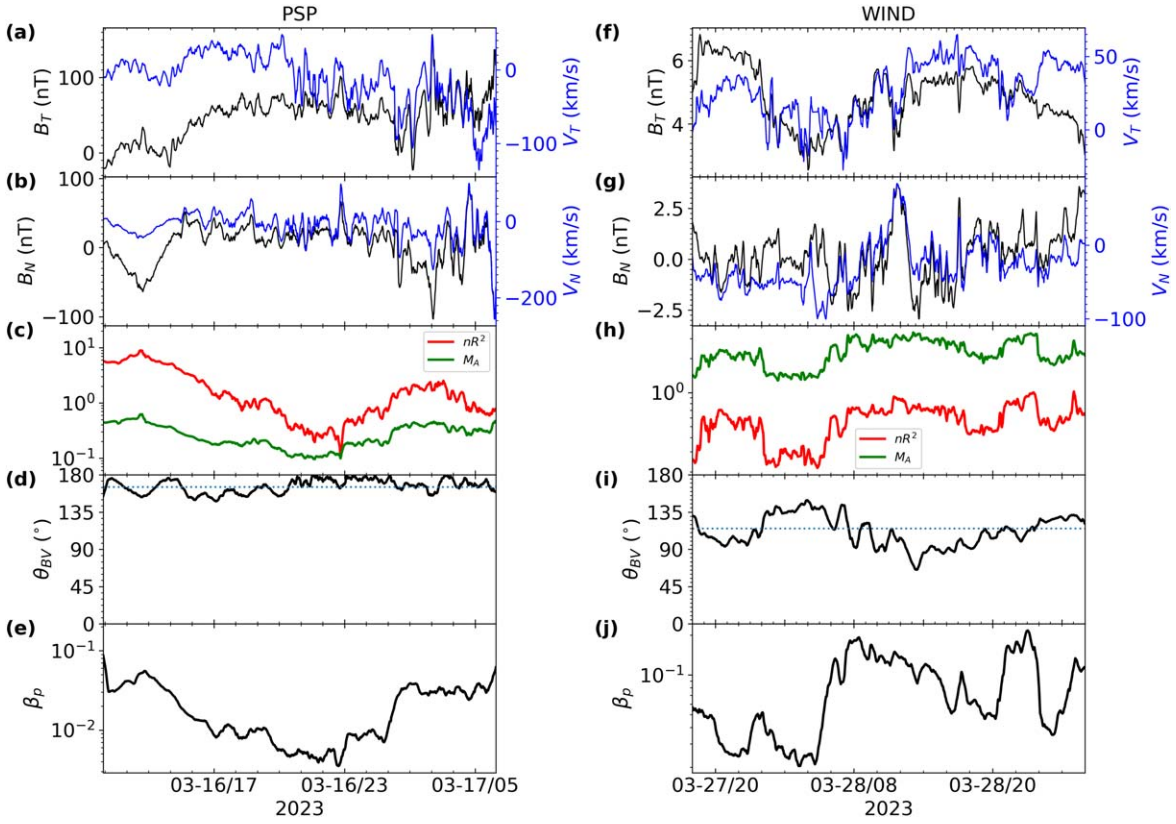

Figure 1. Left panels: time series of the sub-Alfvénic solar wind observed by PSP. Right panels: time series of the modestly super-Alfvénic solar wind observed by Wind spacecraft. (a) and (f) Magnetic field B_T and ion velocity V_T in RTN coordinates. (b) and (g) Magnetic field B_N and ion velocity V_N in RTN coordinates. (c) and (h) Scaled proton number density nR^2 and the Mach number M_A measured by PSP. (d) and (i) Angle between the 30 minutes moving-averaged mean magnetic field and mean plasma velocity, θ_{BV}. The dotted horizontal lines indicates the average values in the corresponding intervals. (e) and (j) Proton plasma beta β_p.

frequency spectra. We then analyze the radial evolution of spectral anisotropy based on the NI MHD theory.

2. Turbulence Evolution from Sub-Alfvénic to Modestly Super-Alfvénic Flows

We use the magnetic field measurements from the PSP/FIELD instrument suite (S. D. Bale et al. 2016) and Wind Magnetic Field Investigation (R. P. Lepping et al. 1995). The ion moments data are from the PSP/SPAN-i instrument (R. Livi et al. 2022) and the 3D plasma analyzer on board the Wind spacecraft (R. P. Lin et al. 1995). Although use of the electron density derived from a quasi-thermal noise (QTN) fit is advised (O. Kruparova et al. 2023), we use the density from SPAN-i instrument due to a large data gap in the QTN data, as done in T. Ervin et al. (2024). We use Welch's method (P. Welch 1967) to calculate the trace power spectra density (PSD). In this method, the whole interval is divided into multiple overlapping subintervals, and the fast Fourier transform is implemented within each subinterval. The subinterval time length is 3.415 hr for PSP data and 13.66 hr for Wind data. The two time lengths are chosen for two reasons. First, because we interpolate the time series to a cadence of 3 s, the 3.415 and 13.66 hr include 4098 and 16392 points, respectively. These point numbers are both powers of two, favoring the implementation of the fast Fourier transform. Second, the frequency resolution allows extensive inertial range to be fitted and multiple subintervals to be averaged.

Figure 1 shows the comparison between the time series of the sub-Alfvénic interval and modestly super-Alfvénic interval. It can be seen that both intervals exhibit high correlations between the magnetic field and velocity fluctuations, implying high Alfvénicity. The M_A ranges from 0.1 to 1 for the sub-Alfvénic flow and from 1.5 to 3.5 for the modestly super-Alfvénic flow. There exists difference in the angle between the mean magnetic field and mean plasma velocity (θ_{BV}) in these two intervals (Figures 1(d) and (i)). For the sub-Alfvénic interval, the average angle $\langle\theta_{BV}\rangle \sim 166°$, implying highly field-aligned flow. For the modestly super-Alfvénic interval, $\langle\theta_{BV}\rangle$ is about 113°, which means the flow is oblique to the mean magnetic field. The plasma betas β_p in these two intervals are all below 0.1 on average, and the PSP interval reaches below a value of $<10^{-2}$ for nearly half the interval period (~6 hr).

Panels (a)–(b) of Figure 2 show the trace PSDs of several quantities for the sub-Alfvénic (left panels) and modestly super-Alfvénic (right panels) intervals, respectively. The Elsässer variables $\boldsymbol{z}^{\pm}$ are defined as $\boldsymbol{z}^{\pm} = \boldsymbol{v} \pm \boldsymbol{b}$, where $\boldsymbol{v} = \boldsymbol{V} - \langle\boldsymbol{V}\rangle$ and $\boldsymbol{b} = (\boldsymbol{B} - \langle\boldsymbol{B}\rangle)/\sqrt{\mu_0\rho_p}$ are the fluctuating velocity and magnetic field. $\boldsymbol{B}$ is the magnetic field, $\boldsymbol{V}$ is the plasma velocity, μ_0 is the permeability of free space, ρ_p is the proton mass density, and $\langle\cdot\rangle$ denotes the ensemble average. It can be seen that the spectral index (α) of the $\boldsymbol{z}^{+}$ spectrum remains unchanged with $\alpha_{z^+}\sim-1.53$, while the z^{-} spectrum steepens indicated by $\alpha_{z^-}\sim-1.35$ at $R \sim 0.08$ au to $\alpha_{z^-}\sim-1.47$ at $R \sim 1$ au. Even though we utilize a power-law fit to the z^{-} spectra here, it is shown below that the z^{-} spectrum is a concave shape consistent with the prediction by the NI MHD theory. Despite not being shown in Figure 2, α_b decreases from

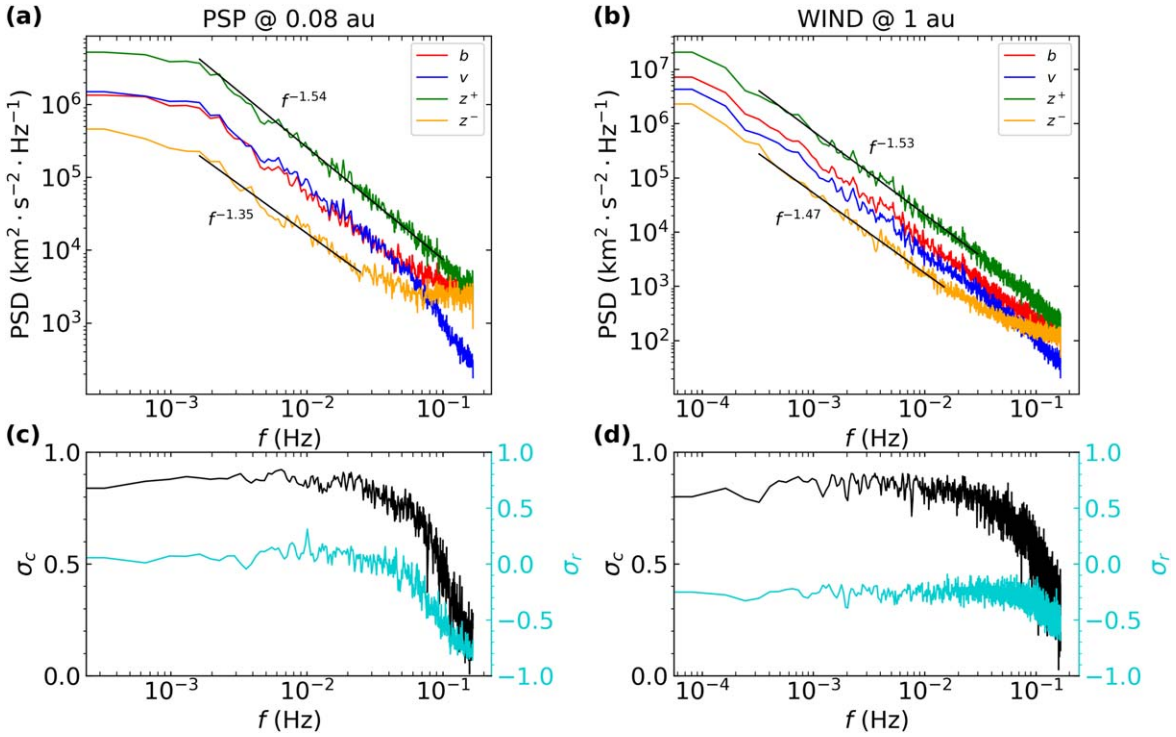

Figure 2. (a) Trace PSDs of a sub-Alfvénic flow observed by PSP. Different colors correspond to the PSD of the velocity v (blue line), the magnetic field in units of fluctuating Alfvén velocity b (red line), and the two Elsässer variables z^+ (green line) and z^- (orange line). The black lines indicate the power-law fits to the z^+ and z^- spectra. (b) Similar to panel (a) but for the Wind observations. (c) Normalized cross helicity (σ_c) and normalized residual energy (σ_r) spectra observed by PSP. (d) σ_c and σ_r spectra observed by Wind spacecraft.

-1.39 to -1.52 while $\alpha_v \sim -1.51$ for both PSP and Wind observations. This indicates that the steepening of z^- is possibly due to the steepening of the magnetic field PSD. The flattening of the z^- spectra at $f > 0.02$ Hz is probably unphysical as a result of the influence of the plasma instrument noise floor (G. P. Zank et al. 2022; H. Wu et al. 2024).

Panels (c-d) show the spectra of the normalized cross helicity $\sigma_c(\equiv(\langle z^+\rangle^2 - \langle z^-\rangle^2)/(\langle z^+\rangle^2 + \langle z^-\rangle^2)))$ and the normalized residual energy $\sigma_r(\equiv(\langle v\rangle^2 - \langle b\rangle^2)/(\langle v\rangle^2 + \langle b\rangle^2)))$. These two parameters denote the power imbalance between z^+ and z^- and v and b, respectively. The average σ_c at $f < 0.01$ Hz is 0.88 and 0.85 for PSP and Wind observations, indicating high-Alfvénicity $\langle z^+\rangle^2 \gg \langle z^-\rangle^2$ for both intervals. However, σ_r has an evident radial evolution. The average σ_r value at $f < 0.01$ Hz is 0.08 for the sub-Alfvénic interval, which indicates that the kinetic fluctuating energy slightly dominates the magnetic field fluctuating energy. Since the Fourier analysis can only reflect the average level, a wavelet analysis is required to verify whether local vortical structures ($\sigma_r > 0$) are present (G. P. Zank et al. 2022), hence leading to an increase of σ_r. Note that this result may possibly also be due to the uncertainty in the plasma moment measurements, which manifest as spikes in the velocity time series, although the σ_c is still close to 1. For the Wind observations, the average σ_r at $f < 0.01$ Hz is -0.25, consistent with previous observations at 1 au (C. H. K. Chen et al. 2013).

In the sub-Alfvénic or modestly super-Alfvénic solar wind, Taylor's hypothesis is no longer valid. Under the usual assumption of stationarity and homogeneity, the observed frequency spectra $P(f)$ in the spacecraft frame is related to the wavenumber spectra $P(\boldsymbol{k})$ by

$$P(f) = \int e^{2\pi f\tau} \int P(\boldsymbol{k}) e^{-i\boldsymbol{k}\cdot\boldsymbol{V}_T} d\boldsymbol{k} d\tau \tag{1}$$

(J. W. Bieber et al. 1996; G. P. Zank et al. 2022). Note that Equation (1) only considers the 1D spatial correlation matrix along the plasma flow direction. A complete description of the observed spectrum associated with the spatial and temporal 4D correlation matrices (L. L. Zhao et al. 2024a, 2024b) should be used in future. J. W. Bieber et al. (1996) proposed a method based on Equation (1) to decompose the observed frequency spectra into 2D and slab components based on the Taylor's hypothesis. Recent work (G. P. Zank et al. 2022) extended this method to the $M_A \lesssim 1$ regime by considering the Doppler effect of the NI/slab fluctuations based on the NI MHD theory (G. P. Zank et al. 2020). The NI MHD theory assumes the $z^\pm$ spectra consisting of a nonpropagating 2D (∞) component and NI/slab ($^*\pm$) components with nonzero frequency caused by the parallel propagation of Alfvén waves. Suppose the 2D component follows a power-law spectrum with spectral index q^∞ (i.e., $P^\infty(f) \sim P^\infty(k_\perp) \sim k_\perp^{-q^\infty}$), the $z^\pm$ spectra $P^{z^\pm}(f)$ can be expressed by the sum of the 2D spectrum $P^\infty(f)$ and the NI/slab spectrum $P\,*\pm(f)$ in the context of NI MHD theory, which are

$$P^{z+}(f) = P^\infty(f) + P^{*+}(f) = C^\infty \left(\frac{U_0 \sin\Psi}{2\pi}\right)^{q^\infty - 1} \times f^{-q^\infty} + C^{*+} \frac{2\pi}{|V_A + U_0 \cos\Psi|} G^{*+}(k_z), \tag{2}$$

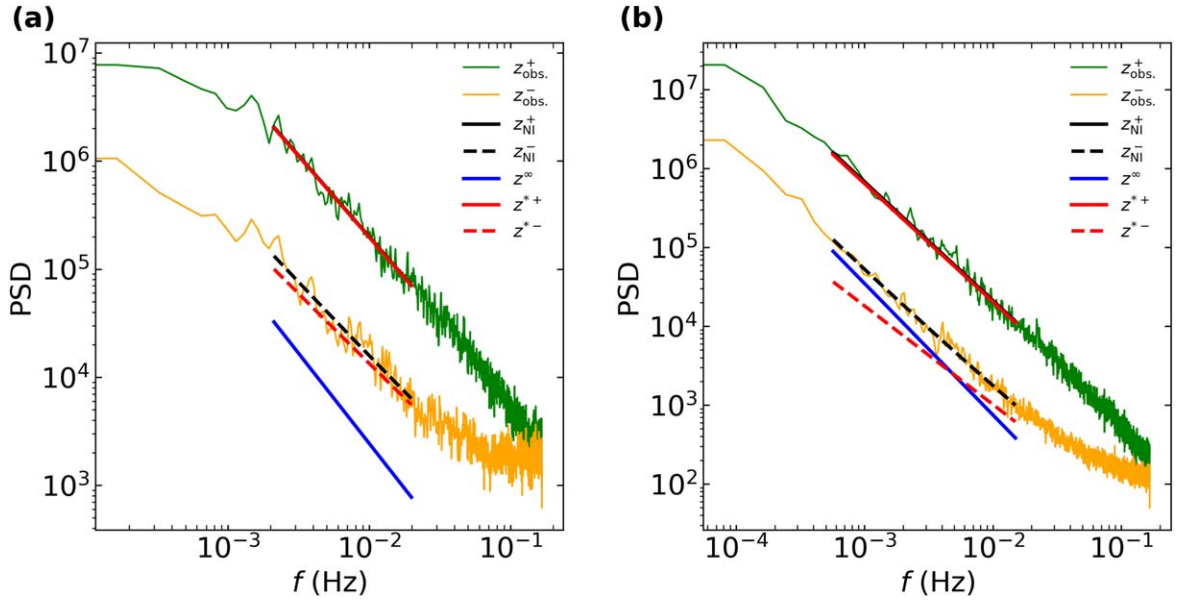

Figure 3. Decomposition of the observed z^+_{obs}. (green) and z^-_{obs}. (orange) spectra into the inferred contribution by the 2D and NI/slab components using the NI MHD theory for (a) sub-Alfvénic and (b) modestly super-Alfvénic solar wind turbulence. The blue solid line represents the inferred 2D turbulence spectrum (z^∞), the red solid line denotes the inferred NI/slab turbulence spectra z^{*+} for z^+, and the red dashed line the inferred NI/slab turbulence spectra z^{*-} for z^-. The black solid line and dashed line are theoretical z^+ and z^- spectra predicted by the NI MHD theory, respectively.

$$P^{z-}(f) = P^{\infty}(f) + P^{*-}(f) = C^{\infty}\left(\frac{U_0 \sin\Psi}{2\pi}\right)^{q^{\infty}-1} \times f^{-q^{\infty}} + C^{*-}\frac{2\pi}{|V_A - U_0\cos\Psi|}G^{*-}(k_z), \quad (3)$$

where C^∞ is the power of the 2D fluctuations and $C*\pm$ is the powers of the forward/backward propagating NI/slab fluctuations. V_A is the Alfvén speed and Ψ is the angle between the background magnetic field $\boldsymbol{B}_0$ and the spacecraft velocity relative to the plasma flow $\boldsymbol{U}_0$, where $\Psi = 14^\circ$ and 67°, respectively. Here, $G^*\pm(k_z)$ is the spectral expression for the NI/slab turbulence in the $\beta_p \ll 1, \sim 1$ regime (Figures 1(e) and (j)), which may not be a power-law spectrum. Following G. P. Zank et al. (2022), we assume $q^\infty = 5/3$, $G^{*+}(k_z) \sim k_z^{-3/2}$, and $G^{*-}(k_z) \sim k_z^{-3/2}(1 + (k_z/k_t)^{0.5})^{0.5}$, where k_t (f_t) is the transition wavenumber (frequency), across which the turbulence cascade transits from a regime dominated by nonlinear interaction to Alfvénic interactions.

We reconstruct the observed frequency spectra using Equation (2) and Equation (3) for both sub-Alfvénic and modestly super-Alfvénic turbulence (Figure 3). The black solid and dashed lines are the $z^\pm$ spectra predicted by the NI MHD theory. The theoretical spectra are well in accord with the observed PSDs. The blue line represents the 2D turbulence spectrum $P^\infty(f)$, and the red lines denote the NI/slab turbulence spectra $P^{*\pm}(f)$. The fit parameters are $C^\infty = 0.094\,\mathrm{km}^{4/3}\ \mathrm{s}^{-2}$, $C^{*+} = 18.981\,\mathrm{km}^{3/2}\ \mathrm{s}^{-2}$, $C^{*-} = 0.557\,\mathrm{km}^{3/2}\ \mathrm{s}^{-2}$, and $f_t = 2.269 \times 10^{-4}$ Hz for the sub-Alfvénic interval and $C^\infty = 0.042\,\mathrm{km}^{4/3}\ \mathrm{s}^{-2}$, $C^{*+} = 2.263\,\mathrm{km}^{3/2}\ \mathrm{s}^{-2}$, $C^{*-} = 0.002\,\mathrm{km}^{3/2}\ \mathrm{s}^{-2}$, and $f_t = 3.287 \times 10^{-10}$ Hz for the modestly super-Alfvénic interval.

In the sub-Alfvénic solar wind, both $P^{z\pm}(f)$ spectra are dominated by the NI/slab fluctuations, as shown in Figure 3(a). In Figure 3(a), the solid blue line shows the inferred 2D mode (z^∞) contribution and the solid red line the inferred highly aligned NI/slab (z^*+) contribution to the observed P(z^+_{obs}.). This dominance arises because the highly aligned magnetic field and flow velocity make NI/slab fluctuations more likely to be observed in the frequency domain compared to 2D fluctuations. Hence, the contribution of the 2D component to the observed spectrum is heavily mediated by the $\sin\Psi$ factor. The contribution of 2D turbulence to the z^- spectrum is evident from the perceptible discrepancy between $P^{z-}(f)$ and $P^{*-}(f)$. For the modestly super-Alfvénic interval (Figure 3(b)), only $P^{z+}(f)$ is predominantly NI/slab fluctuations. $P^{z-}(f)$ contains more 2D fluctuations at lower frequencies, with more NI/Slab fluctuations at higher frequencies. The powers of the 2D and NI/slab components are equal at $f \sim 0.005$ Hz for this modestly super-Alfvénic solar wind turbulence. It is worth noting that the concave shape of the z^- spectrum in G. P. Zank et al. (2022) and L. L. Zhao et al. (2022a) is mainly due to the original shape of the NI/slab spectrum. In our case, however, the magnitudes of $P^\infty(f)$ and $P^{*+}(f)$ are comparable. The superposition of the two different power-law spectra leads to the inertial-range spectrum to be steeper at lower frequencies and flatter at higher frequencies for the z^- spectrum. We note that both fitted f_t s are very low, lying outside the inertial range. This indicates that the inertial-range z^- turbulence is well within the regime where Alfvénic interactions are dominant.

3. Deduction of Spectral Anisotropy for Sub-Alfvénic and Modestly Super-Alfvénic Turbulence

We first test the validity of the modified Taylor's hypothesis for these intervals (K. G. Klein et al. 2015; R. Chhiber et al. 2019). The (modified) Taylor's hypothesis is considered valid if the ratio $\delta V/(V_A + U_0)$ is smaller than 0.1 (R. Chhiber et al. 2019). This ratio is 0.04 and 0.09 for the sub-Alfvénic and modestly super-Alfvénic solar wind flows, respectively. This indicates the violation of the standard Taylor's hypothesis and requires the use of the modified Taylor hypothesis. The ratio of NI/slab and 2D spectra in the frequency domain does not reflect the spectral anisotropy in the wavenumber domain

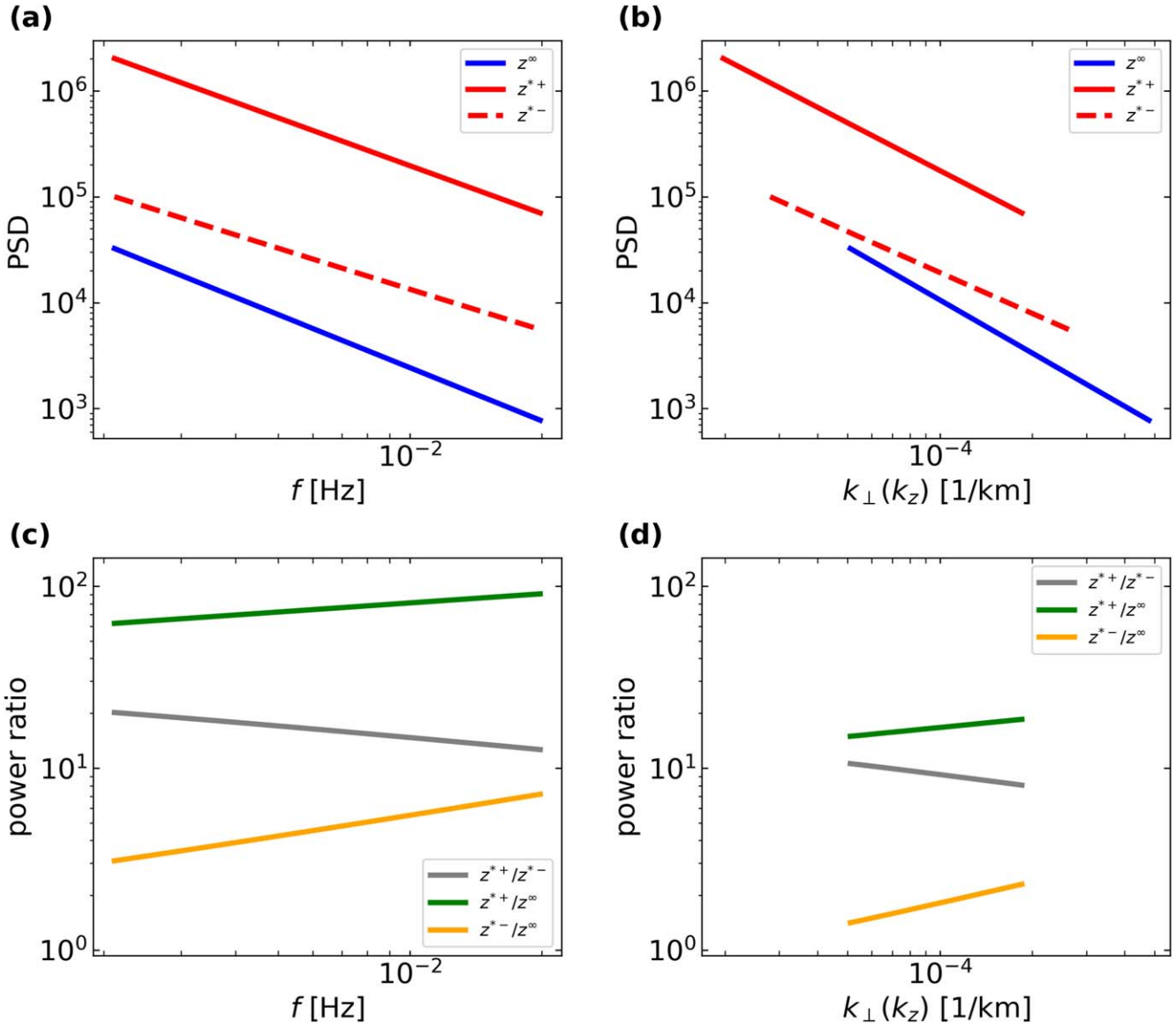

Figure 4. (a) The spacecraft frequency spectra of the inferred contribution of 2D and NI/slab turbulence to the observed spectrum, derived from PSP observations. (b) The wavenumber spectra of the inferred 2D and NI/slab turbulence converted from the frequency spectra. (c) The power ratios of each component in the frequency domain. (d) The power ratios of each component in the wavenumber domain.

(S. Oughton et al. 2015). In addition, it is inappropriate to directly compare C^{∞} and $C^{*}\pm$ because they have different units. To deduce the "true" spectral anisotropy, it is necessary to convert the frequency spectra to wavenumber spectra using the Doppler-shift relations. The corresponding relations between f and $k_z(k_\perp)$ for NI/slab and 2D fluctuations are

$$\begin{aligned} z^{+}&: k_z = 2\pi f/|V_A + U_0\cos\Psi|,\\ z^{-}&: k_z^{*+} = 2\pi f/|V_A - U_0\cos\Psi|,\\ z^{\infty}&: k_\perp^{\infty} = 2\pi f/(U_0\sin\Psi). \end{aligned} \tag{4}$$

Figure 4(a) shows the frequency spectra for the NI MHD components, i.e., $P^{\infty}(f)$ and $P^{*\pm}(f)$ in Figure 3(a). Figure 4(b) shows the converted wavenumber spectra ($P^{\infty}(k_\perp)$, $P^{*\pm}(k_z)$) using Equation (4). It can be seen that, in the same frequency range, the inferred 2D turbulence corresponds to higher wavenumbers, while the inferred forward NI/slab turbulence corresponds to lower wavenumbers. This is expected since the Doppler shift favors outward-propagating waves (M. L. Goldstein et al. 1986; L. L. Zhao et al. 2024a). Figures 4(c)–(d) exhibit the power ratio of different observed components in the frequency domain and wavenumber domain. $P^{*+}(f)/P^{*-}(f)$ (gray line) ranges from 20 to 12 in the frequency range from 0.002 to 0.2 Hz, while the corresponding ratio $P^{*+}(k_z)/P^{*-}(k_z)$ decreases from 10 to 8 (Figure 4(d)) in the common wavenumber range ($5\times10^{-5}\,\mathrm{km}^{-1} < k_z < 2\times10^{-4}\,\mathrm{km}^{-1}$). It is interesting to note that the 2D turbulence is more intense than it appears in the frequency spectra. For example, $P^{*+}(f)/P^{\infty}(f)$ spans from 60 to 90, and $P^{*-}(f)/P^{\infty}(f)$ is in the range of 3–7. However, in the wavenumber domain, $P^{*+}(k_z)/P^{\infty}(k_\perp)$ lies in the range between 15 and 20, and $P^{*-}(k_z)/P^{\infty}(k_\perp)$ decreases to $\sim$2, which is close to isotropic.

Figure 5 shows the same results for the modestly super-Alvénic turbulence. It is worth noting that $P^{*+}(f)/P^{\infty}(f)$ is about 20–30, implying that the observed spectrum is highly NI/slab dominant. Nevertheless, $P^{*+}(k_z)/P^{\infty}(k_\perp)$ drastically decreases to ~ 3, which indicates that the power in the 2D and

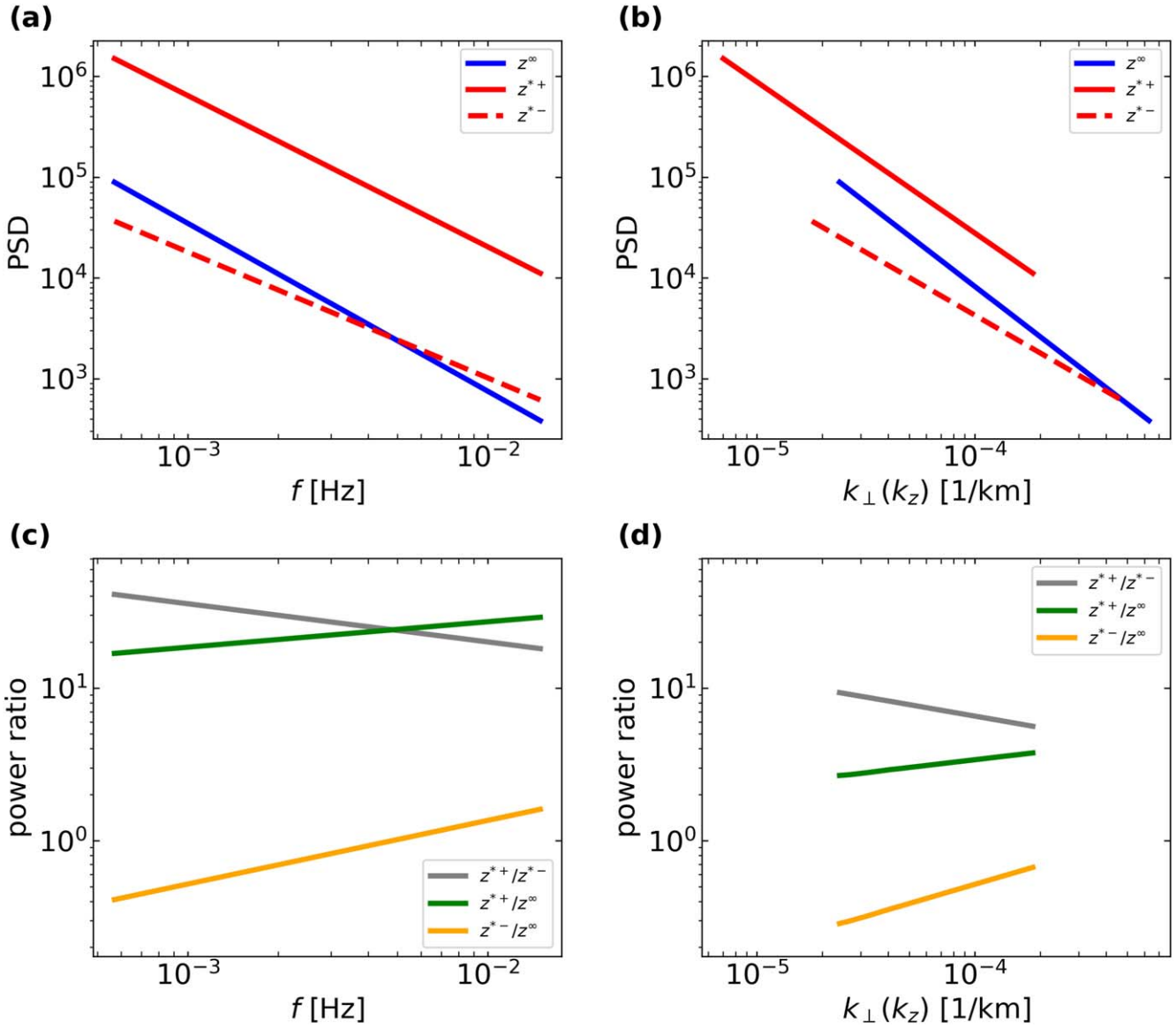

Figure 5. (a) The spacecraft frequency spectra of the inferred contribution of 2D and NI/slab turbulence to the observed spectrum, derived from Wind observations. (b) The wavenumber spectra of the inferred 2D and NI/slab turbulence converted from the frequency spectra. (c) The power ratios of each inferred component in the frequency domain. (d) The power ratios of each component in the wavenumber domain.

NI/slab fluctuations are comparable in the wavenumber range $2.2 \times 10^{-5}\,\mathrm{km}^{-1} < k_z < 2 \times 10^{-4}\,\mathrm{km}^{-1}$. The 2D component is greater than the backward NI/slab component, since the ratio $P^{*-}(k_z)/P^{\infty}(k_\perp)$ lies in 0.3–0.7. $P^{*\pm}(k_z)/P^{\infty}(k_\perp)$ increases with wavenumber for both intervals, suggesting the 2D turbulence is even more intense at larger scales. $P^{*+}(k_z)/P^{\infty}(k_\perp)$ decreases from $\sim$15 at $R \sim 0.08$ au to ~ 3 at $R \sim 1$ au. This indicates that the 2D fluctuations are continuously more important as the solar wind propagates outward.

4. Conclusion

PSP observes a long period of sub-Alfvénic solar wind lasting about 18 hr in the heliocentric distance range 15.6–22 R_S. The "plasma lineup" alignment analysis unveils that the same plasma parcel is possibly also observed by the Wind spacecraft at 1 au. From PSP to Wind locations, the solar wind evolves from sub-Alfvénic to modestly super-Alfvénic. Such a radial alignment provides us a good opportunity to trace the evolution of solar wind turbulence in the same flow, especially for this special case when the solar wind does not evolve to a typical super-Alfvénic ($M_A \gg 1$) state at 1 au. In this work, we study the radial evolution of the MHD turbulence anisotropy by combining the observations from the two spacecraft and the NI MHD theory. We find that, as the solar wind evolves from sub-Alfvénic to modestly super-Alfvénic, the spectral index for z^+ remains unchanged ($\alpha_z^+ \sim -1.53$), while the z^- spectrum steepens with index changing from -1.35 to -1.47. The steepening of the z^- spectrum is related to the steepening of the magnetic field spectrum and potentially the generation of magnetic structures, such as flux ropes and various discontinuities (J. E. Borovsky 2010; G. P. Zank et al. 2017; Y. Chen & Q. Hu 2020; L. L. Zhao et al. 2020, 2021).

We use the NI MHD theory to interpret the observed $z^\pm$ spectra and infer the 2D and NI/slab spectra that contribute to the observed spectra. The spectra predicted by the NI MHD theory well fit the observed spectra. In the frequency domain, the observed inertial-range z^+ spectra for both the sub-Alfvénic

and modestly super-Alfvénic solar wind are dominated by forward-propagating NI/slab fluctuations. The contribution of 2D fluctuations to the observed z^- spectrum is nonnegligible for sub-Alfvénic turbulence, particularly at lower frequencies. Nevertheless, the z^- spectrum in the modestly super-Alfvénic solar wind at 1 au exhibits a slightly concave shape. The power in the 2D and NI/slab fluctuations is comparable, leading to the z^- spectrum being steeper at lower frequencies and flatter at higher frequencies, in contrast to the concave z^- spectra observed in the near-Sun region (G. P. Zank et al. 2022; L. L. Zhao et al. 2022a; H. Wu et al. 2024).

We emphasize that the power anisotropy of the 2D and NI/slab fluctuations in frequency space does not reveal the spectral anisotropy in the wavenumber space, especially in the sub-Alfvénic and modestly super-Alfvénic solar wind. We construct the wavenumber spectra for the 2D and NI/slab turbulence from the observed spectra to analyze the radial evolution of the spectral anisotropy. We find that the inferred 2D fluctuations are more intense than as recorded in the frequency spectra. The ratios $P^{*\pm}(k_z)/P^{\infty}(k_\perp)$ are smaller as compared to their counterparts in the frequency domain, $P^{*\pm}(f)/P^{\infty}(f)$. The power ratio of the inferred forward NI/slab fluctuations and 2D fluctuations $P^{*+}(k_z)/P^{\infty}(k_\perp)$ is $\sim$15 at 0.08 au, while it decreases to $\sim$3 at 1 au. This indicates that more 2D fluctuations are inferred to be present based on the observed spectra as the solar wind propagates outward. This is likely a consequence of the mean magnetic field and mean flow velocity being less aligned, or that 2D fluctuations are increasingly important, or both effects play a role.

The Wind spacecraft at 1 au does not observe a typical Kolmogorov spectrum with a scaling of $f^{-5/3}$, but instead a flatter spectrum with an index of -1.53 is observed. The inferred turbulence anisotropy in the wavenumber domain reveals a slightly greater NI/slab contribution, which is different from the well-known statistical result of an $\sim$80% 2D turbulence contribution for solar wind at 1 au (J. W. Bieber et al. 1996) and the low-β_p NI MHD theory (G. P. Zank et al. 2020). From the PSP to Wind location, the mean proton number density of the flow decreases from 256 to 0.58 cm^{-3}, suggesting a scaling of $n_p \sim R^{-2.4}$. The magnetic field fluctuation energy density $\langle \delta B^2 \rangle$ decreases from 9.7×10^{-10} to 3.6×10^{-13} J, indicating a $\langle \delta B^2 \rangle \sim R^{-3.2}$ scaling. The decay rate of the magnetic field fluctuation energy density is consistent with the Wentzel–Kramers–Brillouin solution prediction that $\langle \delta B^2 \rangle n_p^{\frac{3}{2}} \sim R^{-3.6}$. This implies that the dominant wave-like NI/slab fluctuations are possibly undamped as they propagate outward from 0.08 to 1 au on account of the scarcity of 2D turbulence and/or backward propagating Alfvén modes, therefore ensuring that the nonlinear interactions are retarded (G. P. Zank et al. 2020). This may present a particularly interesting and surprising example of linear Alfvén wave propagation from 0.98 to 1 au in an expanding flow. Using PSP observations, previous works (R. Bandyopadhyay & D. J. McComas 2021; L. L. Zhao et al. 2022a) have investigated the relative contribution of 2D and slab fluctuations using Bieber's method. L. L. Zhao et al. (2022a) found that the power ratio between 2D and slab fluctuations is on average 0.43 (consistent with the result found in the modestly super-Alfvénic interval) when the inertial-range spectral index is observed to be $\sim -3/2$ (C. H. K. Chen et al. 2020). Solar wind turbulence observed by Wind for this particular case is interestingly similar to the turbulence in the near-Sun region due to the observed $-3/2$ spectrum.

Acknowledgments

X.Z., G.P.Z., and L.L.Z. acknowledge the partial support of NASA Parker Solar Probe contract SV4-84017, NSF EPSCoR RII-Track-1 cooperative agreement OIA-1655280, a NASA IMAP subaward under NASA contract 80GSFC19C0027, and NASA awards 80NSSC20K1783 and 80NSSC23K0415. L.L.Z. also acknowledges support by NASA contract 80NSSC23K0415. A.S. is partially supported by NASA grant 80NSSC24K1867. The PSP data used in this Letter are publicly available from NASA's Space Physics Data Facility (SPDF) at https://spdf.gsfc.nasa.gov/pub/data/psp/, and the Wind data are publicly available from https://spdf.gsfc.nasa.gov/pub/data/wind/.

ORCID iDs

Xingyu Zhu https://orcid.org/0000-0002-1541-6397
Gary P. Zank https://orcid.org/0000-0002-4642-6192
Lingling Zhao https://orcid.org/0000-0002-4299-0490
Ashok Silwal https://orcid.org/0000-0001-6286-2106

References

Adhikari, L., Zank, G. P., & Zhao, L. L. 2020, ApJ, 901, 102
Bale, S. D., Goetz, K., Harvey, P. R., et al. 2016, SSRv, 204, 49
Bandyopadhyay, R., & McComas, D. J. 2021, ApJ, 923, 193
Bieber, J. W., Wanner, W., & Matthaeus, W. H. 1996, JGR, 101, 2511
Borovsky, J. E. 2010, PhRvL, 105, 111102
Bourouaine, S., & Perez, J. C. 2018, ApJL, 858, L20
Chandran, B. D. G., & Perez, J. C. 2019, JPlPh, 85, 905850409
Chen, C. H. K., Bale, S. D., Bonnell, J. W., et al. 2020, ApJS, 246, 53
Chen, C. H. K., Bale, S. D., Salem, C. S., & Maruca, B. A. 2013, ApJ, 770, 125
Chen, Y., & Hu, Q. 2020, ApJ, 894, 25
Cheng, W., Liu, Y. D., Ran, H., et al. 2024, ApJ, 967, 58
Chhiber, R., Usmanov, A. V., Matthaeus, W. H., Parashar, T. N., & Goldstein, M. L. 2019, ApJS, 242, 12
Chhiber, R., Pecora, F., Usmanov, A. V., et al. 2024, MNRAS, 533, L70
Cranmer, S. R., & van Ballegooijen, A. A. 2012, ApJ, 754, 92
Duan, D., Bowen, T. A., Chen, C. H. K., et al. 2020, ApJS, 246, 55
Ervin, T., Bale, S. D., Badman, S. T., et al. 2024, ApJ, 972, 129
Goldstein, M. L., Roberts, D. A., & Matthaeus, W. H. 1986, JGR, 91, 13357
He, J., Tu, C., Marsch, E., Bourouaine, S., & Pei, Z. 2013, ApJ, 773, 72
Horbury, T. S., Forman, M., & Oughton, S. 2008, PhRvL, 101, 175005
Kasper, J. C., Klein, K. G., Lichko, E., et al. 2021, PhRvL, 127, 255101
Klein, K. G., Perez, J. C., Verscharen, D., Mallet, A., & Chandran, B. D. G. 2015, ApJL, 801, L18
Kruparova, O., Krupar, V., Szabo, A., Pulupa, M., & Bale, S. D. 2023, ApJ, 957, 13
Lepping, R. P., Acũna, M. H., Burlaga, L. F., et al. 1995, SSRv, 71, 207
Lin, R. P., Anderson, K. A., Ashford, S., et al. 1995, SSRv, 71, 125
Liu, Y. D., Ran, H., Hu, H., & Bale, S. D. 2023, ApJ, 944, 116
Livi, R., Larson, D. E., Kasper, J. C., et al. 2022, ApJ, 938, 138
Matthaeus, W. H., Goldstein, M. L., & Roberts, D. A. 1990, JGR, 95, 20673
Matthaeus, W. H., Zank, G. P., Oughton, S., Mullan, D. J., & Dmitruk, P. 1999, ApJL, 523, L93
Meyrand, R., Squire, J., Mallet, A., & Chandran, B. D. G. 2023, arXiv:2308.10389
Oughton, S., Matthaeus, W. H., Wan, M., & Osman, K. T. 2015, RSPTA, 373, 20140152
Shoda, M., Yokoyama, T., & Suzuki, T. K. 2018, ApJ, 853, 190
Taylor, G. I. 1938, RSPTA, 164, 476
Verdini, A., Velli, M., & Buchlin, E. 2009, ApJL, 700, L39
Welch, P. 1967, IEEE Transactions on Audio and Electroacoustics, 15, 70
Wu, H., Huang, S., He, J., Yang, L., & Yuan, Z. 2024, ApJ, 966, 144
Zank, G. P., Adhikari, L., Hunana, P., et al. 2017, ApJ, 835, 147
Zank, G. P., Adhikari, L., Hunana, P., et al. 2018, ApJ, 854, 32
Zank, G. P., & Matthaeus, W. H. 1992, JGR, 97, 17189
Zank, G. P., & Matthaeus, W. H. 1993, PhFlA, 5, 257

Zank, G. P., Nakanotani, M., Zhao, L. L., Adhikari, L., & Telloni, D. 2020, ApJ, 900, 115
Zank, G. P., Zhao, L. L., Adhikari, L., et al. 2021, PhPl, 28, 080501
Zank, G. P., Zhao, L. L., Adhikari, L., et al. 2022, ApJL, 926, L16
Zhao, L. L., Zank, G. P., Adhikari, L., & Nakanotani, M. 2022a, ApJL, 924, L5
Zhao, L. L., Zank, G. P., Adhikari, L., et al. 2022b, ApJL, 934, L36
Zhao, L. L., Zank, G. P., Adhikari, L., et al. 2020, ApJS, 246, 26
Zhao, L. L., Zank, G. P., Hu, Q., et al. 2021, A&A, 650, A12
Zhao, L. L., Zank, G. P., & Li, H. 2024a, ApJL, 962, L14
Zhao, L. L., Zank, G. P., Opher, M., et al. 2024b, ApJ, 973, 26
Zhu, X., He, J., Verscharen, D., Duan, D., & Bale, S. D. 2020, ApJL, 901, L3